1986ApJ...307..286F

THE ASTROPHYSICAL JOURNAL, 307:286–294, 1986 August 1
© 1986. The American Astronomical Society. All rights reserved. Printed in U.S.A.

AN ANALYSIS OF THE SHAPES OF ULTRAVIOLET EXTINCTION CURVES. I. THE 2175 Å BUMP

EDWARD L. FITZPATRICK[1]
Joint Institute for Laboratory Astrophysics, University of Colorado and National Bureau of Standards

AND

DERCK MASSA[1,2]
Washburn Observatory, University of Wisconsin-Madison
Received 1985 October 14; accepted 1986 January 20

ABSTRACT

IUE data are used to investigate the properties of the 2175 Å interstellar extinction bump toward 45 reddened Milky Way stars. This sample includes stars reddened by some of the most unusual extinction curves observed. Using analytic fitting functions, we derive parameters which describe the central position, FWHM, and strength of the bump. The bump position is very stable, with extreme deviation of only $\sim \pm 17$ Å from the mean position of 2174.4 Å. Nevertheless, this is significantly larger than the measurement uncertainty, indicating a true variability. The bump FWHM has a large range of intrinsic values, 0.77 μm^{-1} (360 Å) to 1.25 μm^{-1} (600 Å). The normalized bump strength, measured as the area under the Lorentzian-like fitting function, varies by more than a factor of 3. There are no convincing correlations among the three bump parameters. However, the width of the bump is strongly correlated with the dust grain environments. Dense quiescent regions (dark clouds and reflection nebulae) yield broad bumps. The diffuse interstellar medium and regions of recent star formation (e.g., the Trapezium) yield narrower bumps.

The absence of any correlation between the bump width and its central position argues strongly against graphite grains in the size range prescribed by the Mathis, Rumpl, and Nordsieck model as the carriers of the bump. Models featuring very small particles (radii ≤ 50 Å) as the bump carriers are more consistent with our results, although the correlation between bump width and dust environment may be difficult to understand.

Subject headings: interstellar: grains — interstellar: matter — line profiles — ultraviolet: spectra

I. INTRODUCTION

The ultraviolet extinction bump at 2175 Å was first detected through rocket observations by Stecher (1965). The ubiquity of the feature and the confirmation of its interstellar origin were demonstrated by Bless and Savage (1972) and Savage (1975) with *OAO 2* satellite spectra. The early observations showed that the strengths of the bump and the far-ultraviolet extinction, relative to $E(B-V)$ and to each other, could vary considerably. More recent studies have now established that such variability is quite common (see Savage *et al.* 1985, and references therein).

The abundant variety of observed ultraviolet extinction curves presents a clear challenge to the development of generalized interstellar grain models, which must be consistent with observations of interstellar abundances, depletions, polarization, and albedo, as well as the extinction. The types of variations seen among different extinction curves certainly provide valuable information regarding the natures of the particles producing the extinction. To exploit this information, it is necessary to understand the detailed behavior of the curves.

This paper is the first in a series whose purposes are to provide a detailed and quantitative description of the shapes of ultraviolet extinction curves, and to uncover the common factors which link them. In addition, we will examine the impact of the codification of curve properties on current models of interstellar grains. This paper exclusively discusses the 2175 Å bump. A parameterization scheme for the bump is presented, and the ranges of the observed parameters are discussed in terms of environmental effects and model predictions. Subsequent papers will examine the relationship between the bump and the other properties of ultraviolet extinction curves (Fitzpatrick and Massa 1986*a*, hereafter Paper II) and collect all the data used in this study and present it in a uniform manner (Fitzpatrick and Massa 1986*b*, hereafter Paper III).

The methodology developed by Massa and Fitzpatrick (1986, hereafter MF) for determining the accuracy to which various extinction parameters may be derived from *IUE* data will be followed in this study.

II. DATA

The extinction curves discussed here were all derived using the "pair method" and are given by

$$k(\lambda - V) \equiv \frac{E(\lambda - V)}{E(B-V)} = \frac{m(\lambda - V) - m(\lambda - V)_{\rm STD}}{(B-V) - (B-V)_{\rm STD}}, \quad (1)$$

where $m(\lambda - V)$ and $B-V$ are the ultraviolet and visual colors of a program star and $m(\lambda - V)_{\rm STD}$ and $(B-V)_{\rm STD}$ are the colors of a dereddened comparison star ("flux standard"). To produce the curves, the energy distributions of each reddened star in our sample and a dereddened comparison star were set in ratio, binned into 0.05 μm^{-1} intervals, converted into magnitudes, and normalized by V and $E(B-V)$.

Our data sets consist of 45 reddened stars and 10 standards. All were observed in the low-resolution mode of the *IUE* satel-

[1] Guest Observer with the *International Ultraviolet Explorer* satellite, which is sponsored and operated by the National Aeronautics and Space Administration, the Science Research Council of the United Kingdom, and the European Space Agency.

[2] Currently at Applied Research Corporation, Landover, Maryland.

© American Astronomical Society • Provided by the NASA Astrophysics Data System

1986ApJ...307..286F

lite with both the SWP and LWR cameras (Boggess *et al.* 1978*a*, *b*). Spectra of many of the reddened stars were obtained from the *IUE* archives through the National Space Science Data Center. Spectra of the standard stars are from the *IUE* spectral atlas of Wu *et al.* (1983). To be included in this study, the reddened stars were required to lie in the spectral type range B5–O6 V–III. Later type stars are excluded because their ultraviolet energy distributions are very strong functions of spectral type—thus amplifying the magnitude of errors associated with spectral mismatching between reddened stars and flux standards. Stars earlier than O6 are not considered because there are no lightly reddened flux standards available. Supergiants and bright giants are also excluded because of the lack of low-dispersion *IUE* observations of unreddened comparison stars and because the B supergiants later than B0.5 have very strong Fe III absorption features in the region 1800–2150 Å. Small mismatches in the strengths of these features between reddened and comparison stars can significantly distort the appearance of 2175 Å bump.

The HD (or BD) numbers, names, spectral types, and $E(B-V)$ values of the reddened stars are listed in Table 1. Other properties of the stars, e.g., distances, visual photometry, etc., will be given in Paper III. It is important to note that these stars do not constitute a random reddening sample. Most were chosen because they lie along lines of sight previously known to produce extinction curves which differ considerably from the Milky Way average. The sources used to assemble this sample are given in the fifth column of Table 1. The original sources of the visual photometry used to compute $E(B-V)$ can be found in these references. We also include a number of stars for which extinction curves have never been published (blank entries in Table 1, fifth col.). Photometry for these stars was taken from the catalogs of Blanco *et al.* (1970) or Nicolet (1978).

The flux standards were all corrected for their small amounts of reddening, using the average Milky Way extinction curve of Seaton (1979) and the intrinsic colors of FitzGerald (1970). The largest $E(B-V)$ value among the standards is 0.07, and these corrections should not significantly affect our results. The standard stars used here, their spectral types, and their optical photometry will be listed in Paper III. The adopted reddening pairs (reddened star plus comparison star) will also be given in Paper III.

In addition to the main 45 star data set, we also include the 33 cluster B stars from MF. The preparation of the extinction curves for these stars is fully described in MF. These data will be used to determine the measurement errors affecting the extinction parameters discussed in § III.

III. PARAMETERIZATION OF THE BUMP

Our analysis of the bump shape will utilize descriptive parameters which result from analytical fits to the bump. The fitting function used to codify the bump and the uncertainties in the various bump parameters are described in this section.

a) The Fitting Function

Savage (1975) first showed, using *OAO 2* spectrometer data, that a Lorentzian function plus a linear, in λ^{-1}, background gives a good fit to the shape of the bump. This result was verified by Seaton (1979) using *TD-1* data and by MF using *IUE* data. In this paper we adopt a slightly different functional form to describe the shape of the bump, which we will refer to as the "Drude" function, or profile. This profile can be understood as an absorption cross section under the assumption of the Drude theory of metals (see Bohren and Huffman 1983, chapter 12). It is easier to interpret physically than a Lorentzian, and it also yields slightly better fits to the data (see below). The complete fitting function, i.e., Drude profile plus linear background, is given by

$$k(\lambda - V) = a_1 + a_2\lambda^{-1} + \frac{a_3}{[\lambda^{-1} - (\lambda_0^{-1})^2/\lambda^{-1}]^2 + \gamma^2}, \quad (2)$$

where λ^{-1} is in units of inverse microns ($\mu\mathrm{m}^{-1}$). Three parameters (λ_0^{-1}, γ, and a_3) define the Drude profile, and two parameters (a_1 and a_2) define the linear background.

The Drude profile parameters characterize the shape and position of the bump. The FWHM (in $\mu\mathrm{m}^{-1}$) of the bump is given by γ, and the position of the bump peak (in $\mu\mathrm{m}^{-1}$) is given by λ_0^{-1}. The strength of the bump can be described in several ways: (1) by the Drude function scale factor, a_3; (2) by the area under the Drude fitting function, given by

$$A = \int_0^\infty \frac{a_3}{[\lambda^{-1} - (\lambda_0^{-1})^2/\lambda^{-1}]^2 + \gamma^2}\, d\lambda^{-1} = \frac{\pi a_3}{2\gamma}; \quad (3)$$

or (3) by the peak intensity of the bump relative to the linear background, given by $a_3/\gamma^2 = 2A/(\pi\gamma)$. This last quantity is most closely related to the $E(\mathrm{BUMP})/E(B-V)$ measurements used by, for example, Savage *et al.* (1985). In the discussion below we adopt A as the measure of bump strength because it is analogous to the concept of equivalent width. However, the other measurements can easily be recovered from the data which will be presented.

Note that relationships between any bump strength measurement and γ are difficult to interpret for two reasons. First, the strength measurements are normalized by $E(B-V)$, and γ is not. Second, each of the strength measures is multiplied by a different power of γ. As a result, one expects that a correlation must appear between one or more of them and γ.

Values of the fitting parameters were determined using standard grid search and linear least-squares procedures to minimize χ^2. The fit was performed in the region 3.3–5.9 $\mu\mathrm{m}^{-1}$, which is symmetric about the nominal bump peak position near 4.6 $\mu\mathrm{m}^{-1}$. Values for λ_0^{-1}, γ, A, a_1, and a_2 are listed in Table 1 for the 45 curves in our main data sample. Mean values and rms scatters per unit $E(B-V)$ for the 45 curve sample are also given, along with mean fit coefficients for each of the five clusters studied by MF. As in MF, these are weighted quantities given by

$$\langle x \rangle = \frac{\sum_{n=1}^{N} x_n E(B-V)_n^2}{\sum_{n=1}^{N} E(B-V)_n^2} \quad (4)$$

and

$$\sigma(x) = \left[\frac{\sum_{n=1}^{N} (\langle x \rangle - x_n)^2 E(B-V)_n^2}{(N-1)}\right]^{1/2}, \quad (5)$$

where x is a bump parameter and N is the number of stars in a given sample.

Figure 1 shows eight examples of the Drude function bump fits and the fit to the overall 45 curve average. The data shown are binned in 0.05 $\mu\mathrm{m}^{-1}$ intervals with the fits superposed. The curves in Figure 1 include some of the most extreme deviations from the Seaton (1979) average curve in our sample. For these curves, and for the entire sample, the Drude fits represent the original data extremely well, without systematic departures.

© American Astronomical Society • Provided by the NASA Astrophysics Data System

1986ApJ...307..286F

TABLE 1

REDDENED STAR AND EXTINCTION CURVE DATA

HD(E) or BD	Name	Spectral Type	E(B-V)	Extinction Curve Source[a]	Bump Parameters λ_0^{-1} (μm^{-1})	γ (μm^{-1})	A (μm^{-1})	Linear Coefficients a_1	a_2 (μm)
13338	...	B1 V	0.51	WBS	4.592	0.931	6.59	-0.06	0.80
14250	Oo1586	B1 III	0.57	...	4.572	0.967	7.00	-0.17	0.77
21483	...	B3 III	0.55	...	4.632	1.018	3.72	-0.27	0.73
34078	AE Aur	O9.5 V	0.53	WBS	4.580	1.016	5.47	0.34	0.63
36982	LP Ori	B2 V	0.34	Pan	4.579	0.908	5.02	1.20	0.01
37022	θ^1 Ori C	O6 p	0.34	BoS	4.633	0.835	2.43	1.24	0.04
37023	θ^1 Ori D	B0.5	0.37	BoS	4.594	0.878	2.18	1.89	-0.09
37061	NU Ori	B0.5 Vp	0.54	Pan	4.572	0.995	2.69	1.24	0.14
37367	...	B2 IV-V	0.40	MSF	4.602	0.908	7.04	0.73	0.54
37903	...	B1.5 V	0.35	MSF	4.616	1.049	5.01	0.98	0.38
38087	...	B3 n	0.33	WBS	4.559	1.000	6.68	1.05	0.26
38131	...	B0.5 V	0.49	WBS	4.604	0.929	5.89	-0.26	0.79
46056	...	O8 Vn	0.51	...	4.607	0.909	4.96	-0.61	0.88
46202	...	O9 V	0.47	...	4.597	0.827	4.63	-0.41	0.89
48099	...	O7 V	0.27	Sea	4.577	0.840	5.70	-0.80	0.86
73882	...	O8.5 V ((n))	0.72	MSF	4.570	1.139	4.12	-0.46	0.81
91824	...	O7 V ((f))	0.27	...	4.605	0.929	5.05	0.24	0.62
93028	...	O9 V	0.24	...	4.625	0.768	2.62	-0.89	0.86
93222	...	O7 III ((f))	0.40	...	4.577	0.807	3.33	-0.06	0.63
147701	...	B5 V	0.73	Sea	4.615	1.136	4.97	1.29	0.33
147888	ρ Oph D	B3 V:	0.52	Sea	4.588	1.026	5.91	1.63	0.13
147889	...	B2 V	1.09	BoS	4.627	1.155	7.14	1.61	0.08
147933/4	ρ Oph AB	B2 IV+V	0.47	BlS	4.596	0.987	5.57	1.69	0.12
149757	ζ Oph	O9.5 V	0.32	BlS	4.579	1.251	5.71	-0.89	0.96
154445	...	B1 V	0.42	Sea	4.562	1.022	7.14	0.99	0.35
167771	...	O7 III:(n)((f))	0.44	Sea	4.563	0.987	5.68	-0.10	0.56
185418	...	B0.5 V	0.50	Sea	4.582	0.951	6.93	1.34	0.33
193322	...	O9 V:((n))	0.41	...	4.610	0.842	4.07	-0.67	0.89
197512	...	B1 V	0.32	WBS	4.579	0.962	6.83	-1.18	1.07
199579	...	O6 V((f))	0.37	Sea	4.610	1.027	4.80	-0.65	0.87
203938	...	B0.5 IV	0.74	Sea	4.587	1.007	5.58	0.07	0.75
204827	...	B0 V	1.11	WBS	4.630	1.124	4.98	-1.44	1.19
229196	...	O6 III(n)(f)	1.22	MSF	4.579	0.974	5.29	-0.22	0.74
239729	...	B0 V	0.66	...	4.602	1.055	4.83	0.04	0.74
251204	...	B1 V	0.78	MSF	4.598	0.921	5.26	-0.57	0.83
252325	...	B0 IV	0.87	MSF	4.621	0.950	5.23	1.15	0.35
+56 524	Oo 1078	B1 Vn	0.60	...	4.576	1.016	6.13	-0.71	0.92
+57 513	...	B1 III	0.54	WBS	4.592	0.929	5.93	-0.84	0.89
+59 562	...	O8 V	0.79	MMN	4.595	0.914	5.21	-0.29	0.75
+60 594	...	O9 V	0.66	MMN	4.596	0.946	5.97	-0.49	0.80
-59 2600	...	O6 V((f))	0.53	...	4.593	0.936	3.97	0.07	0.61
...	Herschel 36	O7.5 V(N)	0.89	HHW	4.619	0.878	3.51	1.66	0.06
...	Hiltner 188	B1 V	0.68	MMN	4.605	0.946	5.68	-1.02	0.97
...	Oo 936	B1.5 V	0.55	...	4.583	0.919	6.20	-0.43	0.91
...	Trumpler 14 #20	O6 V	0.60	...	4.583	0.899	4.10	-0.15	0.72
Mean		...	...	...	4.599	0.992	5.17	0.14	0.62
Standard deviation [per unit E(B-V)]		...	...	...	0.012	0.058	0.71	0.59	0.21
NGC 2244 Mean		...	...	MF	4.597	0.881	5.58	0.07	0.64
NGC 3293 Mean		...	...	MF	4.607	1.006	5.10	0.02	0.69
NGC 6231 Mean		...	...	MF	4.597	0.971	5.58	0.06	0.68
Cepheus OB3 Mean		...	...	MF	4.597	0.989	5.80	0.20	0.61
Trumpler 14 Mean		...	...	MF	4.587	0.981	4.50	0.20	0.54

[a] WBS, Witt *et al.* 1984; Pan, Panek 1983; BoS, Bohlin and Savage 1981; MSF, Massa *et al.* 1983; Sea, Seab 1982; BlS, Bless and Savage 1972; MMN, Morgan *et al.* 1982; HHW, Hecht *et al.* 1982; MF, Massa and Fitzpatrick 1986.

© American Astronomical Society • Provided by the NASA Astrophysics Data System

1986ApJ...307..286F

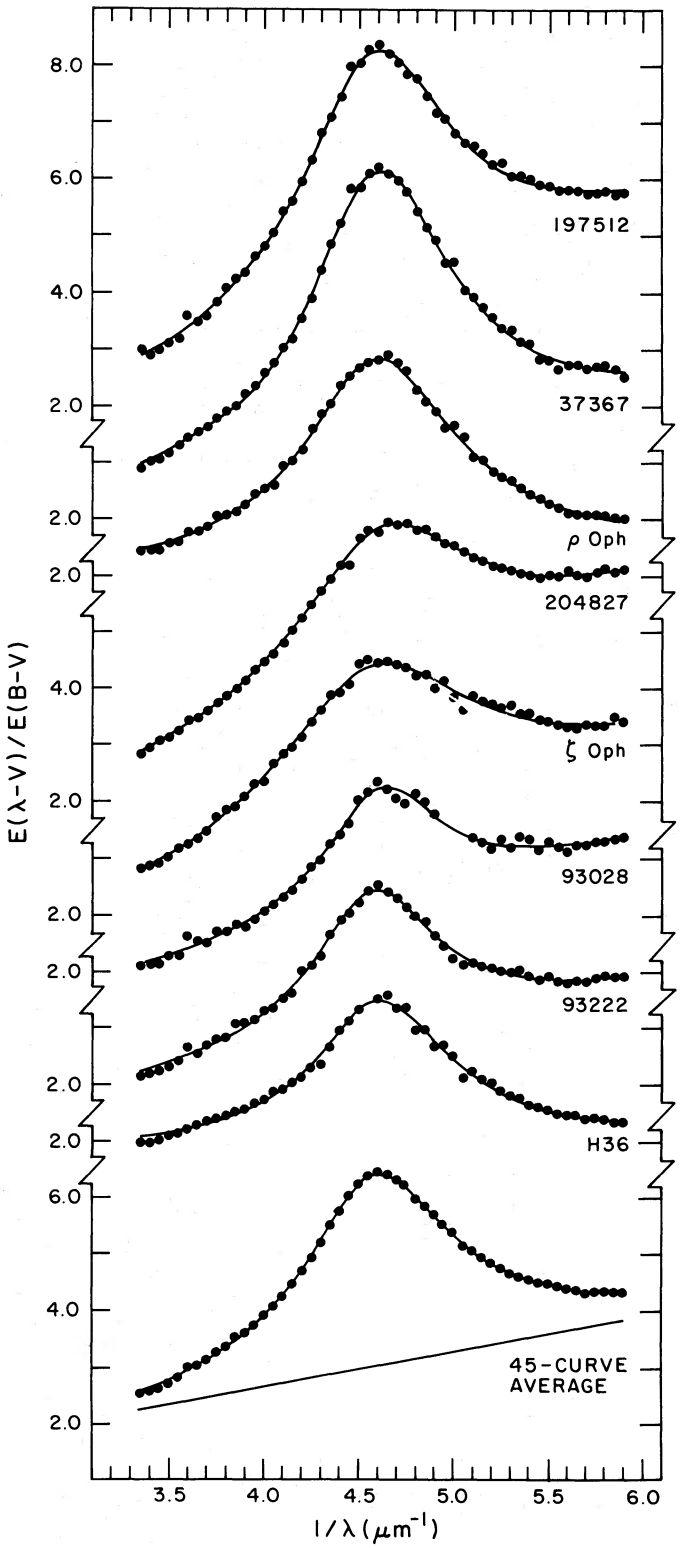

FIG. 1.—Examples of analytical bump fits. The original data, binned in 0.05 Å intervals, are shown for eight curves along with their analytical fits superposed. The 45 curve average, formed by weighting the individual curves by $E(B-V)^2$, and its fit are shown. The linear component of the fit to the average curve is also illustrated.

As shown in MF, Lorentzian profiles also reproduce the observed bumps very well. For our sample, the χ^2 values for the Drude fits are typically only 2%–3% better (smaller) than those for Lorentzian fits, although there are seven cases where the Drude χ^2's are more than 15% better than the Lorentzian values (as opposed to only two cases where the Lorentzian χ^2's are more than 15% better than the Drude values). This is not decisive evidence in favor of the Drude profiles over the Lorentzian profiles. However given that both contain the same number of free parameters and that the Drude profile can easily be interpreted as an absorption cross section—the observed bump is an absorption feature (Witt and Lillie 1973)—we feel that its use is justified. The main difference between the Drude and Lorentzian profiles is that the Drude profile is slightly asymmetric, in the sense that the short-wavelength wing is stronger than the long-wavelength wing (which goes to zero at $\lambda^{-1} = 0\ \mu\text{m}^{-1}$). Consequently, although the parameter λ_0^{-1} obtained from the Drude fit still corresponds to the position of the profile peak, it no longer represents the profile centroid, as it does for a Lorentzian.

b) Uncertainties in the Parameters

i) *Random Error*

In the following sections we compare bump parameters to determine the natures and degrees of variations in bump properties. To make meaningful comparisons, we must know the observational uncertainties affecting bump parameter measurements. This was one of the motivations for the MF study. MF estimated the uncertainties in the parameters by measuring their scatters for stars within clusters or associations believed to have uniform extinction properties. Such determinations provide an upper limit for the measurement errors because there is no guarantee that the extinction toward the clusters is not variable at some level. MF adopted a Lorentzian description of the bump (with a linear background). We have repeated their analysis using the same data set and the Drude profile. The resulting values for the measurement errors (understood to be upper limits) in the parameters γ, λ_0^{-1}, A, a_1, and a_2 are given in Table 2. As in MF, the Cep OB3 data were excluded from all the error estimates except for λ_0^{-1}, because all the other extinction parameters for this cluster appear to vary. Note that the uncertainties are inversely proportional to $E(B-V)$, as might be expected intuitively (although this is only a first-order approximation for γ; see MF).

Since the uncertainties in Table 2 are derived empirically from *IUE* extinction curves, they represent the combined effects of the variety of instrumental uncertainties inherent to *IUE* data and the error introduced by the pair method. These include spectral mismatch error, optical photometry errors, *IUE* photometry errors, and the effects of the *IUE* LWR camera sensitivity change (which affect our analysis in a

TABLE 2

EMPIRICAL UNCERTAINTIES IN BUMP COEFFICIENTS

Coefficient	$\sigma \times E(B-V)$
λ_0^{-1}	0.0059 μm^{-1}
γ	0.021 μm^{-1}
A	0.15 μm^{-1}
a_1	0.17
a_2	0.045 μm

© American Astronomical Society • Provided by the NASA Astrophysics Data System

1986ApJ...307..286F

random manner because the reddened and standard stars in our sample were observed at random times with respect to each other).

In addition to the measurement errors, nonlinearities in the background extinction (which we have assumed to be linear) could also introduce some scatter into the bump parameters. To test the sensitivity of the profile parameters to the choice of background, the bumps were fitted with Drude profiles of fixed γ and λ_0^{-1} (equal to the sample means) and a background consisting of a high-degree polynomial. To fit curves with γ values markedly different from the mean value, the background always assumed the form of a bump or dip roughly symmetric about 4.6 μm^{-1} and sometimes with an area comparable to the Drude profile. These extreme background shapes suggest that the observed range of γ-values is the result of changes in the bump component itself and not the result of variable departures from linearity by the background. The observed variations in the strength of the bump are also clearly properties of the bump component [and the normalizing factor, $E(B-V)$] and not due to background shape variations.

The amplitude of background shape variations required to produce the observed scatter in bump peak positions is much lower than would be required to affect γ or A. However, a very special wavelength dependence, which is antisymmetric about ~ 4.6 μm^{-1}, would be required to shift the profiles and retain the high degree of uniformity in the profile functional forms. The Drude function represents the bumps with extreme values of λ_0^{-1} as well as it represents the rest of the sample. In summary, we think it unlikely that variations in the shape of the background extinction contribute significantly to the scatter observed in the bump profile parameters.

ii) *Systematic Errors*

The presence of low-amplitude, low-frequency curvature in the background cannot be ruled out. If such curvature exists, the measured values of γ, λ_0^{-1}, and A could be systematically different from the "true" values.

We note that our fitting procedure results for γ and λ_0^{-1} are apparently not systematically dependent on the inferred slope of the background extinction. As can be seen from the data in Table 1, there is no evidence for any correlations between the bump parameters and the linear background parameters. Curves with steep or shallow backgrounds can have the same values of λ_0^{-1} and γ (e.g., HD 204827 and HD 147889, or HD 37022 and HD 93028). Also, the fits to the Cep OB3 data from MF show no evidence for λ_0^{-1} variations and only slight evidence for γ variations, despite considerable changes in the background slope.

IV. RESULTS

In this section we evaluate the significance of the scatter observed in the parameters. The data are then examined for correlations with each other and with crude measures of dust environments.

a) Parameter Ranges and Correlations

Figure 2 is a plot of γ (bump FWHM) versus λ_0^{-1} (position of bump peak). Circles represent the 45 curves in the main sample, and squares represent the mean values of the five clusters studied by MF. Error bars on the cluster points indicate the errors in the means. The Cep OB3 point does not have a γ error bar because γ may be variable for this cluster. Error bars representative of an individual measurement [scaled to $E(B-V) = 0.55$] are shown on the right side of Figure 2. The weighted [by $E(B-V)^2$] mean values of the two bump parameters for the 45 curve sample are $\langle\gamma\rangle = 0.992$ μm^{-1} and $\langle\lambda_0^{-1}\rangle = 4.599$ μm^{-1} (2174.4 Å). The relative scatter in bump peak positions is very small. The extreme values are $\lambda_{0\,\max}^{-1} = 4.633$ μm^{-1} (2158 Å) and $\lambda_{0\,\min}^{-1} = 4.559$ μm^{-1} (2193 Å)—a total range of only 35 Å, or less than $\pm 1\%$ from the mean peak

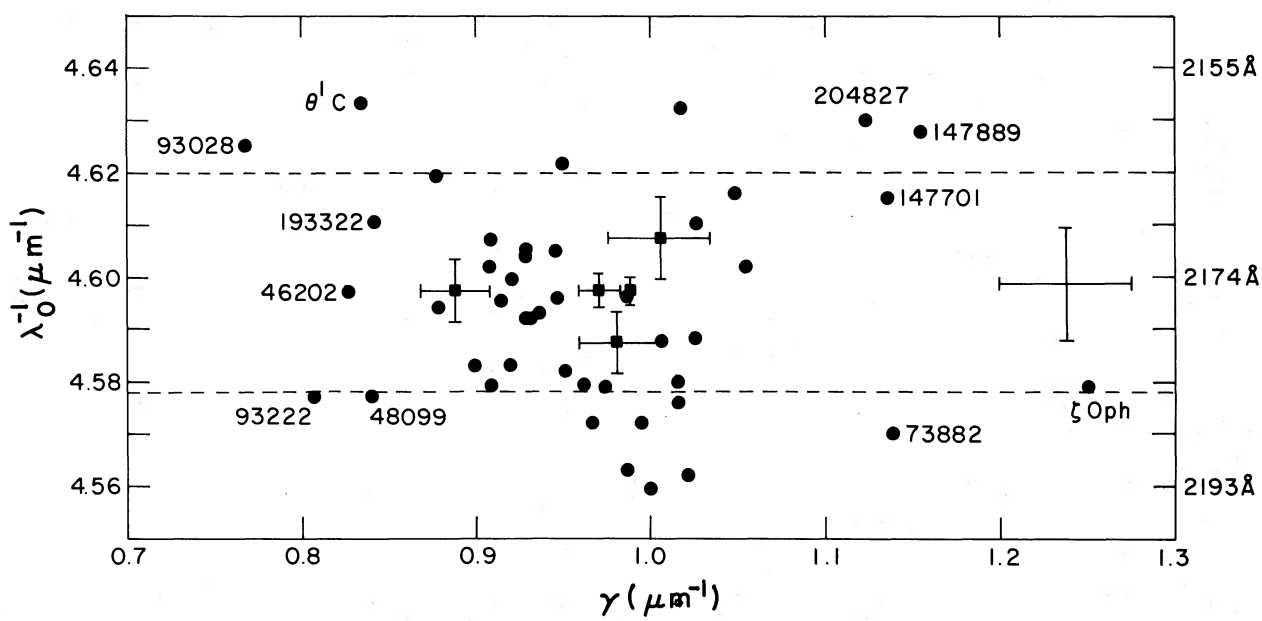

FIG. 2.—Plot of γ (bump FWHM) vs. λ_0^{-1} (bump peak position). *Circles*, data for individual curves. *Squares*, mean values for five clusters studied by MF, with error bars showing the 1 σ uncertainties in the means. No γ error bar is shown for the Cep OB3 point because γ may be variable to this cluster. Error bars representing the 1 σ uncertainty for an individual measurement with $E(B-V) = 0.55$ are shown at the right. *Dashed lines*, ± 2 σ departures from the sample mean for λ_0^{-1} (4.599 μm^{-1}) of a single measurement with $E(B-V) = 0.55$ mag. Points representing curves with the most extreme values of γ are labeled.

© American Astronomical Society • Provided by the NASA Astrophysics Data System

1986ApJ...307..286F

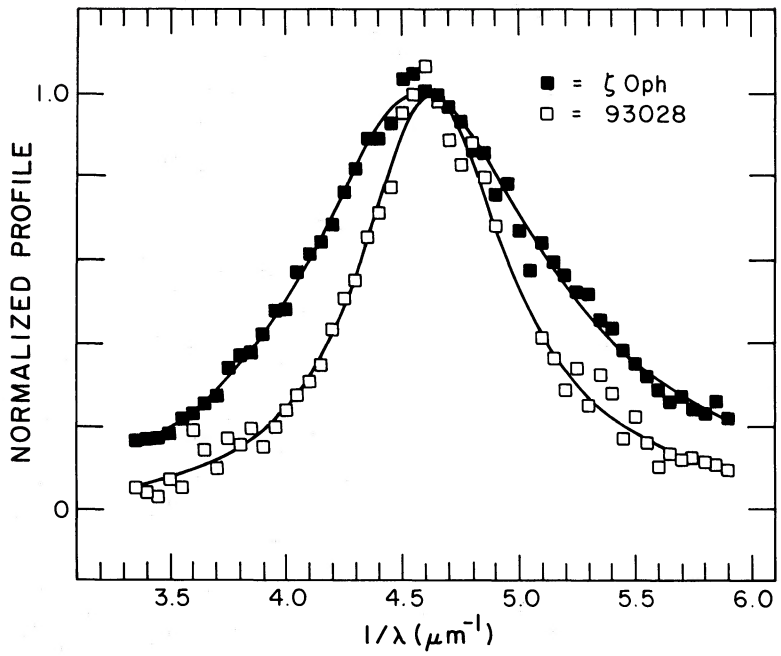

FIG. 3.—Normalized profiles for the broadest and narrowest bumps in our sample. Filled and open symbols represent the binned data for ζ Oph ($\gamma = 1.251\ \mu m^{-1}$) and HD 93028 ($\gamma = 0.768\ \mu m^{-1}$) respectively. Analytical fits are superposed on the data. The linear backgrounds determined from the fitting procedure have been removed and the resultant profiles scaled to the same central peak height.

position. On the other hand, the bump widths range from $\gamma_{max} = 1.251\ \mu m^{-1}$ (597 Å) to $\gamma_{min} = 0.768\ \mu m^{-1}$ (359 Å)—a total range of nearly $\pm 25\%$ from the mean width. Figure 3 illustrates the substantial variation of γ. Normalized bump profiles are shown for the two extreme cases in our sample (the linear backgrounds determined by the fits have been subtracted, and the profiles have been scaled to the same central peak height). Open symbols represent the binned data for HD 93028 ($\gamma = 0.768$), and filled symbols represent the ζ Oph data ($\gamma = 1.251$). The normalized analytical fits to the two bumps are also shown.

We now wish to determine whether the scatter in the parameters obtained from the program curves is significantly larger than the measurement errors determined from the cluster curves. Since MF have already shown that all the parameters except λ_0^{-1} differ significantly from cluster to cluster, we focus our attention on testing the variability of λ_0^{-1}. This can be accomplished by examining the ratio of the variance of the program curves to the variance of the cluster curves. This statistic has an F-distribution with $44 = 45 - 1$ and $28 = 33 - 5$ (MF analyze 33 stars in five clusters) degrees of freedom for the numerator and denominator respectively. Its value is 4.14. The probability that a number this large arises from a sample whose variance is less than or equal to that of the cluster curves is 0.02%. Although this result is subject to the assumption of normally distributed populations, it seems very unlikely that departures from normality could account for such a small probability.

Thus, although it is difficult to single out specific cases with significantly deviant λ_0^{-1} values [only HD 21483, HD 73882, HD 147889, and HD 204827 are more than $\pm 3\sigma(\lambda_0^{-1})/E(B-V)$ from the mean], it is clear that λ_0^{-1} is intrinsically variable for the sample as a whole. As noted in § III*b*(i), we do not believe that background extinction variations contribute significantly to this observed range of λ_0^{-1} values.

If one assumes that the observed variance of our sample is the sum of the squares of the observational and intrinsic scatters, then the intrinsic scatter in λ_0^{-1} is $\sim \pm[(0.0122)^2 - (0.0059)^2]^{1/2}/\langle E(B-V)\rangle = \pm 0.019\ \mu m^{-1}$, or $\sim \pm 9$ Å for $\langle E(B-V)\rangle = 0.55$ mag.

When the F-test is applied to the other parameters, the results are even more dramatic, with all the resulting probabilities being more than 10 times smaller than for λ_0^{-1}, indicating unambiguous intrinsic variability.

The strength of the bump is extremely variable, as has been known for some time. The mean value of the parameter A, the normalized area under the Drude profile, for the 45 curve sample is $\langle A\rangle = 5.17\ \mu m^{-1}$. The total range is 2.2–7.1 μm^{-1}, a variation of more than a factor of 3.

The data in Figure 2 show that there is no evidence of a correlation between γ and λ_0^{-1}. We also find no evidence of a correlation between λ_0^{-1} and normalized bump strength. A marginal correlation between γ and A may exist in our data, in the sense that the narrowest bumps ($\gamma < 0.9\ \mu m^{-1}$) are almost all significantly weaker than the average. The exception is HD 48099. However, this apparent correlation may be just an artifact of our particular sample, since the properties of the HD 48099 curve (i.e., strong, relatively narrow bump) seem to be representative of the Monoceros region in general (e.g., the NGC 2244 stars in MF). For bumps broader than $\gamma = 0.9$, no correlation between γ and A is seen in our data. For the reasons noted in § III, the significance of any correlation between γ and bump strength is difficult to assess.

The linear background coefficients a_1 and a_2 are strongly correlated. This will be discussed in Paper II.

b) *Environmental Effects*

In order to examine how bump properties are influenced by the dust grain environments, we have separated our curves into two groups depending on whether they arise in "diffuse medium" environments or "dense medium" environments.

© American Astronomical Society • Provided by the NASA Astrophysics Data System

1986ApJ...307..286F

TABLE 3

CURVES IN THE "DENSE MEDIUM" GROUP

Curve	Comment
34078 (AE Aur)	Lines of sight pass through reflection nebulae
37903	
38087	
252325	
36982 (LP Ori)	Lines of sight pass through the Orion nebula region
37061 (NU Ori)	
147701	Lines of sight pass through the Sco-Oph dark cloud comples
147888 (ρ Oph D)	
147889	
147933/4 (ρ Oph AB)	
149757 (ζ Oph)	
154445	
21483	From Cohen 1973. Lines of sight probably pass through dark clouds
167771	
185418	
203938	
73882	From Massa *et al.* 1983. Line of sight probably passes through a dark cloud
204827	Large $E(B-V)/r$ value (>2) along the line of sight
37022 (θ^1 Ori C)[a]	Lines of sight pass through the Trapezium
37023 (θ^1 Ori D)[a]	
Herschel 36[a]	Line of sight passes through the M8 complex (Hecht *et al.* 1982)

[a] Located in regions of recent early-type star formation.

The 23 lines of sight in the dense medium group are listed in Table 3. These are directions where much of the observed extinction probably arises in isolated dusty regions, such as reflection nebulae or dark clouds. For the Trapezium stars (θ^1 Ori C and θ^1 Ori D) and Herschel 36, the extinction occurs in regions of recent star formation closely associated with young early-type stars. This type of dense environment is significiantly different from the more quiescent dense regions represented by the dark clouds and reflection nebulae. The properties of the Trapezium and Herschel 36 curves will be considered separately from the rest of the dense medium group.

Figure 4 is a plot of the bump parameters A (Fig. 4*a*), λ_0^{-1} (Fig. 4*b*), and γ (Fig. 4*c*) against $E(B-V)/r$, a measure of the average dust density along the line of sight. [The distances used in the calculations of $E(B-V)/r$ are derived from spectroscopic parallax and will be listed in Paper III.] The mean value of $E(B-V)/r$ for stars within 1 kpc of the Sun is 0.61 mag kpc^{-1} (Spitzer 1978). Although $E(B-V)/r$ itself is not an ideal measure of dust density [e.g., isolated dense regions along otherwise vacant lines of sight will yield misleadingly small $E(B-V)/r$ values], it provides a convenient format for discussing environmental effects. The diffuse medium curves, Trapezium and Herschel 36 curves, and quiescent dense medium curves are represented by filled, half-filled, and open circles respectively. Neither the normalized bump strength A nor the position of the peak λ_0^{-1} appears to be a simple function of environment. (Witt, Bohlin, and Stecher 1984 also found no dependence of bump strength on environmental density.) Figure 4*c* suggests, however, that the observed width of the bump is strongly subject to environmental influences. The curves which have $\gamma > \sim 0.97\ \mu\text{m}^{-1}$ are mostly members of the quiescent dense medium group, while those with $\gamma < \sim 0.97\ \mu\text{m}^{-1}$ are members of the diffuse medium group or the regions with recent star formation. The narrow bumps for the Trapezium and Herschel 36 curves indicate that environmental parameters other than just the dust density may influence the shape of the bump.

V. DISCUSSION

The three significant new results of the current investigation which must be explained by a viable interstellar grain model are: (1) the width γ of the bump varies much more from curve to curve than the position of the bump peak λ_0^{-1} (the extreme ranges are $\pm 25\%$ from the mean value for γ and $\pm < 1\%$ for the mean value for λ_0^{-1}); (2) γ and λ_0^{-1} vary *independently* of one another; and (3) dust in dense quiescent environments produces broad bumps, while dust in the diffuse interstellar medium and in regions of recent early-type star formation produces narrower bumps.

When the 2175 Å bump was first detected, Stecher and Donn (1965) immediately suggested that the feature was produced by interstellar graphite grains. Since that time graphite has become the most widely accepted explanation for the bump. Graphite was incorporated into a quantitative two-component interstellar grain model by Mathis, Rumpl, and Nordsieck (1977, hereafter MRN), which reproduces the mean Milky Way extinction curve very well. The graphite grains in the MRN model follow a power-law size distribution (with an exponent of ~ -3.5) ranging from ~ 50 Å to $\sim 1\ \mu$m in radius. In addition to the bump, graphite in the MRN model also produces the far-ultraviolet upturn seen in Milky Way extinction curves and about half the selective extinction in the visual region. The other half of the selective extinction is provided by silicate grains, the second component of the MRN model. Recently Draine and Lee (1984) showed that the MRN model gives good agreement with observations of extinction in the infrared.

The MRN model is not without its problems. For the particle size range proposed by MRN, both the bump width and position are strong functions of the graphite particle size. The stability of the bump position as observed by Savage (1975; $\lambda_0 = 2175 \pm 30$ Å) then implied that a fairly uniform graphite size distribution must exist over very wide areas of the Galaxy. MRN recognized this problem and suggested that such a ubiquitous size distribution might be the most probable result of the variety of stochastic processes which control interstellar particle size. However, further applications of the MRN model by Mathis and Wallenhorst (1981) were unable to obtain good fits to the bump for a number of "peculiar" extinction curves (θ^1 Ori C, ρ Oph, and σ Sco). The particle size distribution required to fit the extinction at other wavelengths resulted in much broader bumps than observed. Greenberg and Chlewicki (1983) have argued that the apparent independence of the bump strength and the strength of the far-ultraviolet rise rules out the MRN model. Such an independence could probably be achieved in the MRN model through variations in the slope of the size distribution or in the upper and lower size cutoffs. However, the observed constancy of the bump position argues strongly against large fluctuations in the MRN size distribution. Thus, a straightforward implication of our results is that, although graphite cannot be ruled out as the bump carrier, the large intrinsic range of bump widths and the lack of a correlation between bump width and position indicates that the bump *cannot* be dominated by graphite grains in the size range proposed by MRN.

One way to explain the lack of a width-position correlation is to attribute the bump to very small (radii ≤ 50 Å) graphitic

© American Astronomical Society • Provided by the NASA Astrophysics Data System

1986ApJ...307..286F

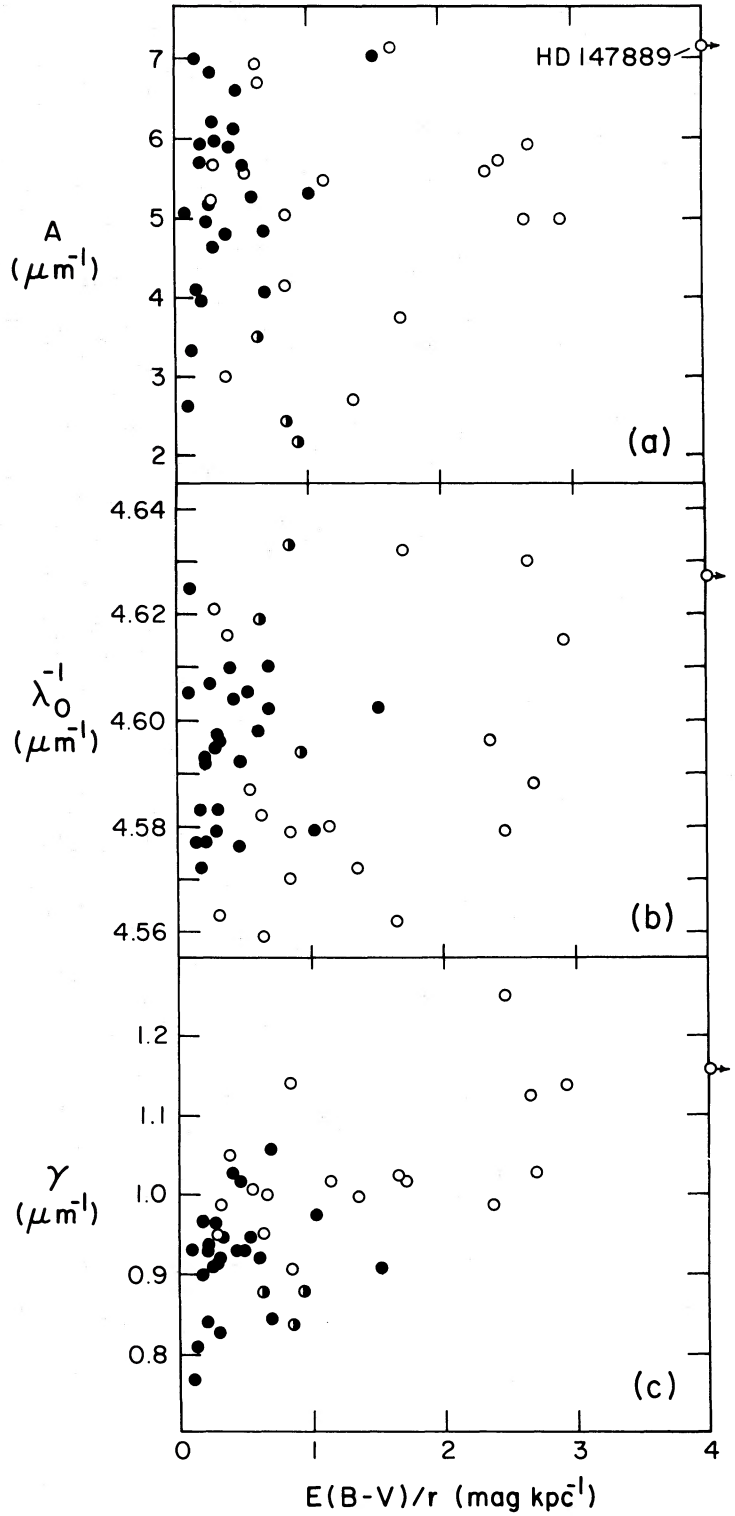

FIG. 4.—Plots of (*a*) A (bump strength), (*b*) λ_0^{-1} (bump peak position), and (*c*) γ (bump FWHM) vs. $E(B-V)/r$. Data for curves from diffuse environments, star-forming environments (Trapezium and Herschel 36 curves), and quiescent dense environments are indicated by filled, half-filled, and open symbols respectively.

© American Astronomical Society • Provided by the NASA Astrophysics Data System

1986ApJ...307..286F

particles, as proposed by Hecht (1986). For an extinction feature produced by such particles, the damping constant in the Drude model (γ in eq. [2]) is inversely proportional to the particle size, while the position of the feature is size-independent (see Bohren and Huffman 1983, chapter 12). A possible shortcoming of this model is that the observed correlation of width and dust density would then imply that dense quiescent regions contain a relative overabundance of the smallest grains compared to the diffuse medium. This seems to conflict with the larger values of R $[=A_v/E(B-V)]$ and $\lambda_{\max}$ (wavelength of maximum polarization) normally measured in such regions. These observations indicate larger than average grain sizes in the dense regions. This may not preclude a small grain component, however, since Witt (1985) has argued that very small particles must be present in the Merope reflection nebula to account for the observed wavelength dependence of the scattered light phase function. Furthermore, there are regions, such as those around the Trapezium and Herschel 36, with large R values—implying larger than average mean grain sizes like the quiescent dense regions—and UV extinction curves with very narrow bumps. Unfortunately, it is impossible, at present, to determine whether the observations which determine R and the bump width arise from the same grain population or from spatially distinct populations along the line of sight. If it could be established that both effects are due to the same grain population, this result would suggest that the processes which affect the bump-producing grains either are different from those which control the grains responsible for R and $\lambda_{\max}$, or else operate on a significantly different time scale.

An alternative quantitative model which naturally explains the environmental correlation is that the bump is due to small graphite grains which form coatings or absorb impurities when immersed in dense environments (Hecht 1986). Very thin amorphous carbon coatings (5 Å on a grain with a $\sim$150 Å radius) change the bump position by only a small amount ($\sim$15 Å) while increasing the FWHM by $\sim$10% (Hecht 1981, private communication). The problem with coatings as an interpretation is to explain why there is such a limited range of coating thicknesses on such a specific range of particle sizes. Otherwise, large shifts in λ_0, with correlated changes in the bump width, are expected to occur. The problem with impurities is that, while hydrogen in the grains might broaden the bump, it cannot be predicted how other impurities might affect the bump width. (See Hecht 1986 for additional details.)

As the previous discussion demonstrates, our results provide valuable constraints on possible interstellar grain models. However, they do not point unambiguously to a specific particle model. Further observational studies, particularly relating bump properties to the dust grain environments and to other observable properties of the grains, will be required to develop an acceptable description of interstellar grain properties.

We are grateful for many helpful discussions with Drs. J. Hecht, J. Mathis, and B. Savage. Much of the data discussed here was acquired from the National Space Science Data Center through Dr. Wayne Warren, Jr. The data were analyzed using the MADRAF facility at the University of Wisconsin-Madison with the helpful assistance of Marilyn R. Mead. D. M. was supported by National Aeronautics and Space Administration grant NAGW-283, and E. F. by National Science Foundation grant AST 83-12964.

REFERENCES

Blanco, V. M., Demers, S., Douglass, G. C., and FitzGerald, M. P. 1970, *Pub. US Naval Obs.*, **21**.
Bless, R. C., and Savage, B. D. 1972, *Ap. J.*, **171**, 293.
Boggess, A., *et al.* 1978*a*, *Nature*, **275**, 372.
———. 1978*b*, *Nature*, **275**, 377.
Bohlin, R. C., and Savage, B. D. 1981, *Ap. J.*, **249**, 109.
Bohren, C. F., and Huffman, D. R. 1983, *Absorption and Scattering of Light by Small Particles* (New York: Wiley-Interscience).
Cohen, J. G. 1973, *Ap. J.*, **186**, 149.
Draine, B. T. and Lee, H. M. 1984, *Ap. J.*, **285**, 89.
FitzGerald, M. P. 1970, *Astr. Ap.*, **4**, 234.
Fitzpatrick, E. L., and Massa, D. 1986*a*, in preparation (Paper II).
———. 1986*b*, in preparation (Paper III).
Greenberg, J. M., and Chlewicki, G. 1983, *Ap. J.*, **272**, 563.
Hecht, J. 1981, *Ap. J.*, **246**, 794.
———. 1986, *Ap. J.*, **305**, 000.
Hecht, J., Helfer, H. L., Wolf, J., Donn, B., and Pipher, J. L. 1982, *Ap. J. (Letters)*, **263**, L39.
Massa, D., and Fitzpatrick, E. L. 1986, *Ap. J. Suppl.*, **60**, 305 (MF).
Massa, D., Savage, B. D., and Fitzpatrick, E. L. 1983, *Ap. J.*, **266**, 662.
Mathis, J. S., Rumpl, W., and Nordsieck, K. H. 1977, *Ap. J.*, **217**, 425 (MRN).
Mathis, J. S., and Wallenhorst, S. G. 1981, *Ap. J.*, **244**, 483.
Morgan, D. H., McLachlan, A., and Nandy, K. 1982, *M.N.R.A.S.*, **198**, 779.
Nicolet, B. 1978, *Astr. Ap. Suppl.*, **34**, 1.
Panek, R. J. 1983, *Ap. J.*, **270**, 169.
Savage, B. D. 1975, *Ap. J.*, **199**, 92.
Savage, B. D., Massa, D., Meade, M., and Wesselius, P. R. 1985, *Ap. J. Suppl.*, **59**, 397.
Seab, C. G. 1982, Ph.D. thesis, University of Colorado.
Seaton, M. J. 1979, *M.N.R.A.S.*, **187**, 73P.
Spitzer, L. 1978, *Physical Processes in the Interstellar Medium* (New York: Wiley-Interscience), p. 156.
Stecher, T. P. 1965, *Ap. J.*, **142**, 1683.
Stecher, T. P., and Donn, B. 1965, *Ap. J.*, **142**, 1681.
Witt, A. N. 1985, *Ap. J.*, **294**, 216.
Witt, A. N., Bohlin, R. C., and Stecher, T. P. 1984, *Ap. J.*, **279**, 698.
Witt, A. N., and Lillie, C. F. 1973, *Astr. Ap.*, **25**, 397.
Wu, C.-C., *et al.* 1983, *IUE Ultraviolet Spectral Atlas, IUE NASA Newsletters*, No. 22.

EDWARD L. FITZPATRICK: Joint Institute for Laboratory Astrophysics, University of Colorado, Boulder, CO 80309-0440

DERCK MASSA: Applied Research Corporation, 8201 Corporate Drive, Suite 920, Landover, MD 20785

© American Astronomical Society • Provided by the NASA Astrophysics Data System